Effects of Micro-Scale Mobility and Beam Misalignment in On-Body mmWave Systems

Asad Ali, *Member, IEEE*, Olga Galinina, *Member, IEEE*, Jiri Hosek, *Senior Member, IEEE*, and Sergey Andreev, *Senior Member, IEEE*

***Abstract*— Wearable devices positioned on a human body have challenges in millimeter-wave (mmWave) communication due to micro-scale mobility, such as subtle shakes and rotations. These movements can compromise the radio link performance. It may be problematic for high-rate immersive applications, where this can lead to substantial degradation in the user's quality of experience. In this letter, we propose a framework to quantify the impact of micro-scale mobility and beam misalignment on the performance of on-body mmWave links. Our findings reveal that for varying levels of beam misalignment, it is possible to adjust the antenna half-power beamwidth to enhance the data rates.**

***Index Terms*— Beam misalignment, micro-scale mobility, personal wearable devices, millimeter-wave communication.**

I. Introduction

ONE of the envisioned 5G/6G scenarios [1] involves the support of mobile augmented reality (AR) and mixed reality (MR) applications. These can be deployed on wearable devices, such as AR glasses, tethered to a device with better computing capabilities and longer battery life, such as a smartphone, tablet, or puck. The resulting network of interconnected wearable devices located in close proximity to an individual – referred to as a wearable Personal IoT Network (PIN) [2] – is expected to offer users higher data rates at lower latency and increased network capacity for AR/MR applications. As a result, PINs enable a seamless immersive experience, while the computing device serves dual roles as a processing unit and a gateway providing IP connectivity.

The microwave frequency band lacks the capacity to meet the demands of future immersive applications [3]. A more suitable alternative is the millimeter-wave (mmWave) frequency band, which offers a larger bandwidth and extremely high data rates. However, the use of highly directional mmWave antennas can lead to beam misalignment, which occurs when a directional beam deviates from the intended receiver due to changes in the relative distance and orientation of antennas caused by micro-scale user mobility, such as smaller shakes and rotations [4]. Beam misalignment can potentially lead to disruptions in the operation of the emerging rate-hungry services [5] if not compensated for by frequent beamforming procedures.

Most research efforts were focused on studying the effects of beam misalignment in medium- and long-range links, such as in [5] and [6], while there has been limited exploration of directionality effects for short-range on-body communications. The impact of highly directional connectivity was studied in the context of terahertz (THz) networks [7] and [8]. In our previous work [9], we examined the system-level performance of mmWave PINs by considering off-body interference. However, micro-scale mobility and beam misalignment were only addressed in the context of off-body communication [4]. A comparison of the state-of-the-art is summarized in Table I.

In on-body mmWave systems, the relative positions and orientations of the antennas may deviate considerably between transmissions, as also observed in [10], which can result in a substantial decrease in antenna gain, hence impacting the received signal strength. For shorter links, micro-mobility and beam misalignment are the primary sources of randomness and data rate fluctuations. Consequently, understanding the impact of these factors on on-body mmWave systems is instrumental to optimizing their performance and selecting better radio settings.

In this letter, we aim at analyzing the effects of random beam misalignment and micro-scale mobility on mmWave link performance. Our contributions can be summarized as follows:

- We propose a novel theoretical framework for on-body mmWave systems that incorporates arbitrary distributions of beam misalignment and micro-scale mobility of a wearable device. We provide analytical expressions for the distribution of the data rate.
- We conduct numerical analysis to study the interplay between the transmit power, antenna beamwidth, micro-scale mobility, beam misalignment, and the resulting data rate.
- We provide insights on reducing the data rate fluctuations and enhancing the data rates by appropriately selecting the transmit power and antenna beamwidth.

The proposed framework can serve as a valuable tool for other researchers and practitioners by enabling further in-depth mathematical analysis, theoretical sensitivity assessment, and reduction of data rate fluctuations caused by micro-mobility.

II. System Model

A. User Model and Device Placement

We consider a scenario where a user is equipped with advanced wearable technology, such as AR glasses, and a

Manuscript received 26 October 2023; revised 5 December 2023; accepted 24 December 2023. Date of publication 2 January 2024; date of current version 12 March 2024. This work was supported by the H2020 A-WEAR ITN/EJD and by the Academy of Finland (projects RADIANT, IDEA-MILL, and SOLID). The associate editor coordinating the review of this letter and approving it for publication was A. Li. *(Corresponding author: Asad Ali.)*

Asad Ali and Sergey Andreev are with the Unit of Electrical Engineering, Tampere University, 33720 Tampere, Finland, and also with the Department of Telecommunications, Brno University of Technology, 61600 Brno, Czech Republic (e-mail: asad.ali@tuni.fi; sergey.andreev@tuni.fi).

Olga Galinina is with the Tampere Institute for Advanced Study, Tampere University, 33100 Tampere, Finland (e-mail: olga.galinina@tuni.fi).

Jiri Hosek is with the Department of Telecommunications, Brno University of Technology, 61600 Brno, Czech Republic (e-mail: hosek@vut.cz).

Digital Object Identifier 10.1109/LCOMM.2023.3349349

TABLE I
STATE-OF-THE-ART COMPARISON

	This work	[5]	[6]	[8]	[9]	[10]	[4]
Misalignment	✓	✓	✓	✓	×	×	✓
Micro-mobility	✓	×	×	×	×	✓	✓
Variable rate	✓	✓	✓	✓	×	✓	✓
On-body comms.	✓	×	×	×	✓	×	×

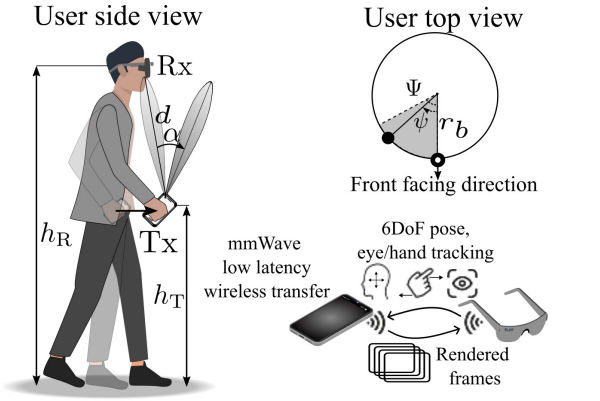

Fig. 1. User micro-scale mobility and beam misalignment.

companion computing device, referred to as the Rx and the Tx, respectively. The user is modeled as a cylinder with a fixed radius of r and height of h_{B}. The Tx and Rx devices are placed on the surface of the cylinder at fixed heights of h_{T} and h_{R}, respectively. The position of the Rx determines the front-facing direction of the user, and the Tx is placed such that its projection onto the 2D plane is located at an angular distance ψ from the Rx projection. We consider an arbitrary truncated distribution $f_\psi(\psi)$ of angle ψ, with the range limited to $[\Phi_{\min}, \Phi_{\max}]$. To reflect the forward placement of the Tx device, we intentionally limit the maximum angle $\Phi_{\max}$ to $\frac{\pi}{2}$. The employed geometrical abstraction is illustrated in Fig. 1.

B. Directional Connectivity

The devices are considered to be wirelessly tethered, thereby forming a wearable PIN. They communicate using a directional medium access control protocol with omnidirectional reception, e.g., IEEE 802.11ad/ay. We assume that Tx forms a directional 3D beam, which is axially symmetric around the antenna boresight and has no side lobes due to antenna tapering. The degree of directivity is determined by the half-power beamwidth (HPBW), θ, measured at the half-power or -3 dB point of the main lobe of the beam.

The gain of the antenna array is approximated by a product of two components: the maximum directivity gain $G_{\max}$ achieved by a transmission along the antenna boresight and the directivity reduction factor $\rho(\alpha)$ corresponding to a gain decrease due to the deviation α from the axis, such that $G_{\mathrm{tx}} = G_{\max} \cdot \rho(\alpha)$. Here, α represents the angle between the antenna beam boresight and the direct path from the Tx to the Rx, which we regard as the *angle of beam misalignment*. We also allow α to follow an arbitrary truncated distribution $f_\alpha(\alpha)$ with its range limited to $[0, \alpha_{\max}]$.

The maximum achievable directionality gain is estimated as a ratio between the area covered by a directional beam on a sphere and the surface area of a sphere, which may be expressed as $G_{\max} = \frac{2}{1-\cos\frac{\theta}{2}}$. Coefficient $\rho(\alpha)$ is determined by the antenna radiation pattern in 3D space and can be approximated as suggested in [11]:

$$\rho(\alpha) = 1 - \frac{\alpha}{\theta}, \quad \alpha \le \theta. \tag{1}$$

C. Received Signal Power and Data Rate

Let d denote the 3D distance between the devices. Then, the average path gain can be modeled as:

$$g(d) = Ld^{-\gamma}, \tag{2}$$

where L and γ are referred to as the propagation constant and the propagation exponent for the on-body channel, respectively. The reception is assumed to be omnidirectional, e.g., $G_{\mathrm{rx}} = 1$; therefore, for $\alpha \ge 0$, the received power at the Rx can be calculated as a function of the transmit power P_{tx} as

$$P_{\mathrm{rx}}(d,\alpha) = P_{\mathrm{tx}} G_{\mathrm{tx}} G_{\mathrm{rx}} g(d) = P_{\mathrm{tx}} G_{\max} \left(1 - \tfrac{\alpha}{\theta}\right) L d^{-\gamma}. \tag{3}$$

Using the Shannon-Hartley theorem, we can estimate the data rate $\tilde{r}$ as follows:

$$\tilde{r} = w \log\left(1 + \mathrm{SNR}\right), \tag{4}$$

where w is the bandwidth, SNR is the signal-to-noise ratio (SNR) defined as $\mathrm{SNR} = \frac{P_{\mathrm{rx}}}{P_{\mathrm{n}}}$ with P_{n} representing the noise power.

Notably, in practical systems, the maximum achievable data rate (denoted as r_{SNR}) is dependent on the selected modulation and coding scheme (MCS). The MCS defines a combination of modulation and error-correction coding used for wireless data transmission, thereby determining the maximum achievable data rate. Higher MCS levels with more sophisticated modulation and coding enable higher maximum data rates. As a result, the upper limit on the data rate can be expressed as $r_{\mathrm{SNR}} = w \log\left(1 + \mathrm{SNR}_{\max}\right)$, where $\mathrm{SNR}_{\max}$ is the SNR level corresponding to the selected MCS. Consequently, the *effective* data rate is obtained as $r = \max(\tilde{r}, r_{\mathrm{SNR}})$.

In the following section, we explore the performance of mmWave links in a wearable PIN during an immersive AR session. Particularly, we contribute an expression that allows one to obtain the mean data rate for arbitrary distributions of angle ψ defining the position of a wearable device and angle α characterizing the beam misalignment.

III. ON-BODY mmWAVE PERFORMANCE EVALUATION

In this section, we derive an expression for the distribution of the data rates on on-body directional links that can incorporate various distributions of micro-scale changes in the antenna position and beam misalignment. We employ the transformation of random variables and distribution marginalization techniques to obtain our sought distribution.

The distribution of the central angle, $f_\psi(\psi)$, characterizes the position of the Tx when transmitting data to the Rx for an AR application. For a user at a fixed height, we express the distance between the Rx and the Tx as a function of the central angle ψ at the center of the user, as shown in Fig. 1. With this distribution, we can obtain the distribution of distances between the devices, which can then be used along with the distribution of beam misalignment angles to obtain

the distribution of the data rate. We first express the distance between the Rx and the Tx as follows:

$$d(\psi) = \sqrt{4\ r_{\mathrm{b}}^2 \sin^2\left(\frac{\psi}{2}\right) + d_v^2}, \tag{5}$$

where $d_v = h_{\mathrm{T}} - h_{\mathrm{R}}$ is the vertical distance between the devices.

According to our system model, the central angle ψ can range between $\Psi_{\min}$ and $\Psi_{\max}$, which implies that the on-body distance d between the devices ranges between $d = d_{\min} = d(\Psi_{\min})$ and $d = d_{\max} = d(\Psi_{\max})$. With these definitions, we can proceed to derive the expressions that allow to numerically calculate our target metrics of interest.

The data rate r is dependent on the distance d between the devices and the beam misalignment α. We may express the data rate r as a function of distance d and beam misalignment α as $r = w \log\left(1 + \frac{P}{d^\gamma}\left(1 - \frac{\min(\alpha,\theta)}{\theta}\right)\right)$, where $P = \frac{P_{\mathrm{tx}} G_{\max} L}{P_{\mathrm{n}}}$ is introduced for brevity.

The data rate $\tilde{r}$ without the r_{SNR} limit ranges from the minimum data rate $\tilde{r}_{\min} = r\left(d_{\max}, \alpha_{\max}\right)$, where the distance is the longest and the misalignment is maximum, to the maximum data rate $\tilde{r}_{\max} = r\left(d_{\min}, 0\right)$, where the distance is the shortest and the beams are perfectly aligned.

Proposition: For arbitrary truncated distributions of the beam misalignment angle $f_\alpha(\alpha)$ and the central angle $f_\psi(\psi)$, the distribution of the data rate without the MCS-imposed limit $f_{\tilde{r}}(\tilde{r})$ can be expressed as

$$\begin{aligned} f_{\tilde{r}}(\tilde{r}) = {} & \frac{2(1-C_0)P^{2\gamma-1}\theta e^{\frac{\tilde{r}}{w}}}{\gamma w C_r \left(\theta(e^{\tilde{r}/w}-1)\right)^{1+2/\gamma}} \int_0^{\min(\alpha(\tilde{r},d_{\min}),\theta)} f_\alpha(\alpha) \\ & \times f_\psi\left(2\arcsin\left(\tfrac{1}{2r_b}\sqrt{z(\tilde{r})-d_v^2}\right)\right) \\ & \times \frac{(\theta-\alpha)^{2/\gamma-1}\left(\theta d^\gamma\left(e^{\tilde{r}/w}-1\right)+P(\theta-\alpha)\right)}{\sqrt{\left(z(\tilde{r})-d_v^2\right)\left(d_v^2-z(\tilde{r})+4r_b^2\right)}}\mathrm{d}\alpha \\ & + C_0\delta(\tilde{r}), \tilde{r} \in [\tilde{r}_{\min}, \tilde{r}_{\max}], \end{aligned} \tag{6}$$

where the coefficient $C_r = F_{r,0}(r_{\max}) - F_{r,0}(r_{\min})$ and the coefficient $C_0 = F_\alpha(\max(\theta, \alpha_{\max})) - F_\alpha(\theta)$.

Proof: The data rate $\tilde{r}$ depends on the angle of misalignment α and the distance d, subject to the placement of Tx determined by the internal angle ψ. However, it is essential to address the situation of complete beam misalignment ($\alpha > \theta$), which leads to a transmission failure with $\tilde{r} = 0$. To quantify the probability of the event where $\alpha > \theta$, we introduce the coefficient C_0, which can be calculated as

$$C_0 = \int_\theta^{\max(\theta,\alpha_{\max})} f_\alpha(\alpha)\mathrm{d}\alpha = F_\alpha(\max(\theta,\alpha_{\max})) - F_\alpha(\theta). \tag{7}$$

Consequently, the distribution of the data rate $\tilde{r}$ becomes a mixture of a discrete distribution and a continuous distribution, due to the fact that for $\alpha > \theta$, the data rate $\tilde{r}$ is zero. The probability density function (PDF) of this mixture can be obtained as

$$f_{\tilde{r}}(\tilde{r}) = f_{\tilde{r},0}(\tilde{r})(1-C_0) + C_0\delta\left(\tilde{r}\right), \tag{8}$$

where $f_{\tilde{r},0}(r)$ is the distribution function for $\tilde{r} > 0$ without the r_{SNR} limit and $\delta\left(\tilde{r}\right)$ is the Dirac delta function at $\tilde{r} = 0$. To derive the expression for $f_{\tilde{r},0}(\tilde{r})$, we marginalize the joint distribution $f_{\tilde{r},\alpha}(\tilde{r},\alpha|\alpha \le \theta)$. By marginalizing, we integrate over all possible values of α that satisfy the condition $\alpha \le \theta$. Hence, in the remainder of this work, the conditional part of this notation is omitted for brevity, and the joint distribution is then presented as $f_{\tilde{r},\alpha}(\tilde{r},\alpha)$.

To obtain the joint distribution $f_{\tilde{r},\alpha}(\tilde{r},\alpha)$, we employ a bivariate transformation represented by the following expression:

$$f_{\tilde{r},\alpha}(\tilde{r},\alpha) = f_{\psi,\alpha}(\psi(\tilde{r},\alpha),\alpha)|J| = f_\psi(\psi(\tilde{r},\alpha))f_\alpha(\alpha)|J|, \tag{9}$$

where $|J|$ is the absolute value of the determinant for the Jacobian matrix. For the considered transformation, the latter is given as

$$\begin{aligned} |J| &= \begin{vmatrix} \frac{\partial\psi(\tilde{r},\alpha)}{\partial\tilde{r}} & \frac{\partial\psi(\tilde{r},\alpha)}{\partial\alpha} \\ \frac{\partial\alpha(\tilde{r},d)}{\partial\tilde{r}} & \frac{\partial\alpha(\tilde{r},d)}{\partial\alpha} \end{vmatrix} \\ &= \frac{\partial\psi(\tilde{r},\alpha)}{\partial\tilde{r}}\frac{\partial\alpha(\tilde{r},d)}{\partial\alpha} - \frac{\partial\psi(\tilde{r},\alpha)}{\partial\alpha}\frac{\partial\alpha(\tilde{r},d)}{\partial\tilde{r}}. \end{aligned} \tag{10}$$

By utilizing the joint distribution $f_{\tilde{r},\alpha}(\tilde{r},\alpha)$ given by (9), we can derive $f_{\tilde{r},0}(\tilde{r})$ by marginalizing it with respect to α. The resulting expression is then:

$$\begin{aligned} f_{\tilde{r},0}(\tilde{r}) = {} & \int_0^{\min(\alpha(\tilde{r},d_{\min}),\theta)} f_\psi(\psi(\tilde{r},\alpha))f_\alpha(\alpha)|J|\mathrm{d}\alpha \\ = {} & \frac{2P^{2/\gamma-1}\theta e^{\frac{\tilde{r}}{w}}}{\gamma w C_r\left(\theta(e^{\tilde{r}/w}-1)\right)^{1+2/\gamma}} \int_0^{\min(\alpha(\tilde{r},d_{\min}),\theta)} f_\alpha(\alpha) \\ & \times f_\psi\left(2\arcsin\left(\tfrac{1}{2r_b}\sqrt{z(\tilde{r})-d_v^2}\right)\right) \\ & \times \frac{(\theta-\alpha)^{2/\gamma-1}\left(\theta d^\gamma\left(e^{\tilde{r}/w}-1\right)+P(\theta-\alpha)\right)}{\sqrt{\left(z(\tilde{r})-d_v^2\right)\left(d_v^2-z(\tilde{r})+4r_b^2\right)}}\mathrm{d}\alpha, \tilde{r} \in [\tilde{r}_{\min}, \tilde{r}_{\max}], \end{aligned} \tag{11}$$

where the coefficient $C_r = F_{\tilde{r},0}(\tilde{r}_{\max}) - F_{\tilde{r},0}(\tilde{r}_{\min})$.

Notably, the expression for $F_{\tilde{r},0}(\tilde{r})$ is as follows:

$$\begin{aligned} F_{\tilde{r},0}(\tilde{r}) = {} & \frac{2P^{2/\gamma-1}}{\gamma w\theta^{2/\gamma}} \int_{\tilde{r}_{\min}}^{\tilde{r}} \frac{e^{\frac{x}{w}}}{(e^{x/w}-1)^{1+2/\gamma}} \int_0^{\min(\alpha(x,d_{\min}),\theta)} f_\alpha(\alpha) \\ & \times f_\psi\left(2\arcsin\left(\tfrac{1}{2r_b}\sqrt{z(x)-d_v^2}\right)\right) \\ & \times \frac{(\theta-\alpha)^{2/\gamma-1}\left(\theta d^\gamma\left(e^{x/w}-1\right)+P(\theta-\alpha)\right)}{\sqrt{\left(z(x)-d_v^2\right)\left(d_v^2-z(x)+4r_b^2\right)}}\mathrm{d}\alpha\mathrm{d}x, \tilde{r} \in [\tilde{r}_{\min}, \tilde{r}_{\max}]. \end{aligned} \tag{12}$$

By substituting (11) into (8), we arrive at the distribution of the data rate without the r_{SNR} limit, which can be expressed as (6). ∎

Since the data rate without the r_{SNR} limit $\tilde{r}$ can range between $\tilde{r}_{\min}$ and $\tilde{r}_{\max}$, it is possible that the SNR at the Rx is greater than $\mathrm{SNR}_{\max}$. In this case, the data rate $\tilde{r}$ is limited to the maximum achievable data rate r_{SNR} corresponding to the selected MCS. Therefore, the effective data rate r after considering the limitation imposed by the MCS ranges from $r_{\min} = \min\left(\tilde{r}_{\min}, r_{\mathrm{SNR}}\right)$ to $r_{\max} = \min\left(\tilde{r}_{\max}, r_{\mathrm{SNR}}\right)$.

Theorem: For any truncated distribution of the beam misalignment angle $f_\alpha(\alpha)$ and the central angle $f_\psi(\psi)$, the

distribution of the effective data rate $f_r(r)$ may be given as

$$f_r(r) = \frac{2(1-C_0)(1-C_s)P^{2\gamma-1}\theta e^{\frac{r}{w}}}{\gamma w C_r \left(\theta(e^{r/w}-1)\right)^{1+2/\gamma}} \int_0^{\min(\alpha(r,d_{\min}),\theta)} f_\alpha(\alpha) \times f_\psi\left(2\arcsin\left(\frac{1}{2r_b}\sqrt{z(r)-d_v^2}\right)\right) \times \frac{(\theta-\alpha)^{2/\gamma-1}\left(\theta d^\gamma\left(e^{r/w}-1\right)+P(\theta-\alpha)\right)}{\sqrt{(z(r)-d_v^2)\left(d_v^2-z(r)+4r_b^2\right)}}\mathrm{d}\alpha + (1-C_s)C_0\delta(r) + C_s\delta(r-r_{\text{SNR}}), r \in [r_{\min}, r_{\max}], \quad (13)$$

where $C_s = F_{\tilde{r},0}(r_{\max}) - F_{\tilde{r},0}(r_{\min})$ is a scaling coefficient.

Proof: Considering the effective data rate, any values $\tilde{r} \geq r_{\text{SNR}}$ are replaced with a fixed data rate $r = r_{\text{SNR}}$. As a result, the distribution of the data rate r can be obtained as a mixture of two distributions: the Dirac delta distribution $\delta(r - r_{\text{SNR}})$ and the distribution $f_{\tilde{r}}(r)$. Hence, the resulting distribution may be represented as

$$f_r(r) = f_{\tilde{r}}(r)(1-C_s) + C_s\delta(r-r_{\text{SNR}}), \quad r \in [r_{\min}, r_{\max}], \quad (14)$$

where $C_s = F_{\tilde{r},0}(\tilde{r}_{\max}) - F_{\tilde{r},0}(r_{\max})$ is a coefficient representing the probability that $\tilde{r} \geq r_{\text{SNR}}$. ∎

We can now derive our metrics of interest by using the distribution $f_r(r)$. For any distribution function of the beam misalignment angle $f_\alpha(\alpha)$ and the central angle $f_\psi(\psi)$, the expected data rate can be obtained as $E[r] = \int_{r_{\min}}^{r_{\max}} r f_r(r)\mathrm{d}r$. Additionally, this expression may be used to calculate the standard deviation of the data rate as $\sigma_r = \sqrt{E[r^2] - E[r]^2}$. Our framework enables the incorporation of micro-scale mobility, as characterized by the movement of devices and modeled by the internal angle ψ, and of beam misalignment, as modeled by the misalignment angle α. The derived distribution can be employed for further mathematical analysis and optimization, which may be challenging to achieve with simulations only.

IV. Numerical Results and Discussion

In this section, we present our numerical results to illustrate the impact of various parameters. We consider a user equipped with AR glasses (Rx) and an accompanying processing unit (Tx). Both devices are wirelessly paired to each other via a direct directional mmWave link using IEEE 802.11ay radio technology. We require the Tx to be on the front side of the user's torso and assume to have the line of sight to the Rx. We also utilize the log-distance pathloss model from [13] and adapt it to $g(d) = Ld^{-\gamma}$ pathloss format. For simulations, we use realistic antenna radiation patterns obtained from MATLAB's `sensorArrayAnalyzer` app for uniform rectangular array (URA) antennas. For the results obtained from our analytical expressions, we utilize θ that corresponds to the HPBW of the URA radiation pattern (e.g., $\theta = 30$ corresponds to 4×4 URA). Specifically, the analytical results utilize the antenna pattern obtained by using (1). The parameters employed in this section are summarized in Table II.

We assume that the Tx position, which is determined by the central angle ψ, follows a truncated normal distribution with the mean μ_ψ and the standard deviation σ_ψ, having its range limited to $[0, \frac{\pi}{2}]$. To address misalignment, we introduce a variable x, which follows a truncated normal distribution with the mean $\mu_\alpha = 0$ and the standard deviation σ_α. The misalignment angle is then defined as $\alpha = |x|$, thus resulting in a folded distribution centered at zero with the range of $[0, \pi]$. While our framework can incorporate different distributions, we use these examples for the sake of exposition.

TABLE II
Notation and Parameters of Our Numerical Study

Parameter	Value	Parameter	Value
User radius, r_b	0.15 m	Max SNR, $\text{SNR}_{\max}$	17 dB [12]
Height of Rx, h_{R}	1.75 m	Prop. constant, L	71.2 [13]
Height of Tx, h_{T}	0.9 m	Prop. exponent, γ	4.1 [13]
Transmit power, P_{tx}	20 dBm	Antenna type	URA
Carrier frequency, f	60 GHz	Antenna element	Cosine
Carrier bandwidth, w	2.16 GHz	Cosine power	2
Noise power, P_N	-74 dBm	Element spacing	0.4λ

In Fig. 2a, we present the standard deviation of the data rate σ_r with respect to the increasing deviation in the central angle μ_ψ for different Tx positions and transmit powers. Here, μ_ψ represents the mean position of the Tx and σ_ψ is the degree of variation in the Tx position (e.g., during sitting, walking, running, etc.). From Fig. 2a, we learn that an increase in the value of σ_ψ leads to a corresponding growth for the standard deviation of the data rate σ_r.

In statistics, an empirical rule states that for a normal distribution, 99.7% of values lie within $3\sigma_r$ of the $E[r]$. For the standard deviation of the data rate σ_r, the value of the data rate can also change by $3\sigma_r$ around the mean data rate $E[r]$, e.g., with a standard deviation of 125 Mbps, it is possible to have a drop of up to 375 Mbps around the mean data rate. Immersive applications are characterized by both high data rates and stringent packet delay budgets (PDBs); hence, significant fluctuations in the data rate can result in exceeding the PDB and thereby failing to satisfy the user's expectations. Additionally, we observe that higher transmit power leads to a wider deviation in the data rate. Furthermore, as the Tx moves away (e.g., by increasing μ_ψ), the deviation of the data rate grows for higher σ_ψ and vice versa for lower σ_ψ. We conclude that employing a Transmit Power Control (TPC) mechanism to lower the power can help reduce fluctuations in the data rate.

In Fig. 2b, we display the mean data rate $E[r]$ with respect to an increasing misalignment σ_α for different numbers of antenna elements (HPBW) and transmit powers. In practice, the value of σ_α can be impacted by various factors, including the angular and displacement velocities of the antenna, the employed beamforming algorithm, and the size of the antenna array. Essentially, these factors influence the beam realignment delay in response to changes in the antenna location and orientation. For a shorter realignment delay, the value of σ_α is expected to be small.

We compare our analytical results obtained from (1) with the simulation results using realistic antenna patterns. Fig. 2b shows that with a growing misalignment, there is a corresponding decline in the data rate. We observe that wider beams are more robust as the data rate decreases gradually for an increasing misalignment as compared to narrower beams. The performance improvement from larger numbers of antenna elements for narrow beams diminishes as the data rate

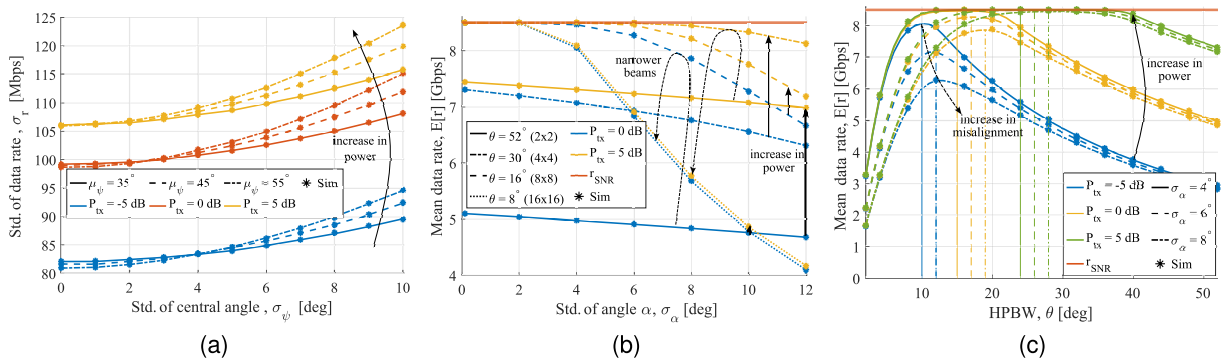

Fig. 2. Impact of micro-scale mobility and beam misalignment on data rate in on-body communication. (a) Standard deviation of rate w.r.t. σ_ψ. (b) Mean data rate vs. σ_α. (c) Mean data rate vs. HPBW.

approaches r_{SNR}. As the power grows and the beams become narrower, the data rate saturates at r_{SNR} imposed due to MCS.

We also observe that under a lower transmit power, when the standard deviation of the misalignment angle σ_α increases, antennas with higher numbers of elements perform better than those with lower numbers of elements, provided that the mean data rate $E[r]$ for the perfectly aligned beams ($\sigma_\alpha = 0$) is not equal to r_{SNR}. Narrow beams and high transmit powers typically lead to improved data rates. However, for a higher transmit power, antennas with fewer antenna elements (wider beams) can outperform those with higher numbers of elements (narrow beams) in terms of the data rate due to beam misalignment. Narrower beams are more susceptible to misalignment, thus, making wider beams preferable in the cases of strong misalignment, such as during increased user movement. This leads to an important insight that applying a TPC mechanism in situations with a high degree of beam misalignment may benefit from using higher transmit power.

In Fig. 2c, we present the mean data rate with respect to an increasing beamwidth θ for a varying standard deviation of the misalignment angle σ_α. The simulation results (depicted by $*$) are provided alongside the analytical results using the beam pattern given by (1) instead of the realistic patterns obtained from MATLAB's `sensorArrayAnalyzer`. We consider a large range of values, including those that do not directly correspond to the number of antenna elements.

Knowing the statistical aspects of the beam misalignment can help deliver higher data rates. This knowledge can be highly beneficial in improving the system performance when coupled with an adaptive beamwidth control algorithm, wherein the HPBW can be adjusted by partially deactivating the antenna array [14]. For the antenna arrays with a limited number of antenna elements, such as those in devices like smart AR glasses, the achievable HPBW is constrained, thus, simplifying the selection of HPBW.

V. Conclusion

In this letter, we propose a novel framework for evaluating the performance of on-body mmWave systems in the presence of micro-scale mobility of wearable devices and beam misalignment. Our methodology incorporates arbitrary distributions modeling the positions of wearable devices and beam misalignment angles. Our results demonstrate that increasing the transmit power can effectively mitigate the performance decline caused by beam misalignment, albeit with higher fluctuations in the data rate. Additionally, the findings highlight that the HPBW of an antenna array can be appropriately adjusted with statistical knowledge of the beam misalignment for any selected transmit power to achieve higher data rates. Wider beams prove advantageous in the scenarios with a high degree of misalignment, i.e., during increased user movement. Our analysis can aid in selecting the transmit power and the HPBW values that deliver better performance when employing a TPC mechanism and adaptive beamwidth control algorithms.

References

[1] *Support of 5G Glass-Type Augmented Reality/Mixed Reality (AR/MR) Devices (Release 18)*, document TR 26.998, V18.0.0, 3GPP, 2023.
[2] *Study on Tethering AR Glasses*, document TR 26.806, V18.0.0, 3GPP, Architectures, QoS and Media Aspects (Release 18), 2023.
[3] J. Begole, "Immersive reality: Opening new kinds of interactive experiences," Huawei Technol.Tech. Rep., 2015.
[4] V. Petrov et al., "Capacity and outage of terahertz communications with user micro-mobility and beam misalignment," *IEEE Trans. Veh. Technol.*, vol. 69, no. 6, pp. 6822–6827, Jun. 2020.
[5] A. Thornburg and R. W. Heath, "Ergodic capacity in mmWave ad hoc network with imperfect beam alignment," in *Proc. IEEE Mil. Commun. Conf.*, Oct. 2015, pp. 1479–1484.
[6] E. N. Papasotiriou et al., "Performance analysis of THz wireless systems in the presence of antenna misalignment and phase noise," *IEEE Commun. Lett.*, vol. 24, no. 6, pp. 1211–1215, Jun. 2020.
[7] W. Chen et al., "Enhancing THz/mmWave network beam alignment with integrated sensing and communication," *IEEE Commun. Lett.*, vol. 26, no. 7, pp. 1698–1702, Jul. 2022.
[8] Z. Ding and H. V. Poor, "Design of THz-NOMA in the presence of beam misalignment," *IEEE Commun. Lett.*, vol. 26, no. 7, pp. 1678–1682, Jul. 2022.
[9] A. Ali et al., "Performance evaluation of dynamic computation offloading capability for industrial wearables," in *Proc. IEEE 32nd Annu. Int. Symp. Pers., Indoor Mobile Radio Commun. (PIMRC)*, Sep. 2021, pp. 1–7.
[10] K. Turbic et al., "A mobility model for wearable antennas on dynamic users," *IEEE Access*, vol. 6, pp. 63635–63648, 2018.
[11] O. Chukhno et al., "Analysis of 3D deafness effects in highly directional mmWave communications," in *Proc. IEEE Global Commun. Conf. (GLOBECOM)*, Dec. 2019, pp. 1–6.
[12] C. R. da Silva et al., "Analysis and simulation of the IEEE 802.11ay single-carrier PHY," in *Proc. IEEE Int. Conf. Commun. (ICC)*, May 2018, pp. 1–6.
[13] R. Aminzadeh et al., "WBAN channel modeling for 900 MHz and 60 GHz communications," *IEEE Trans. Antennas Propag.*, vol. 69, no. 7, pp. 4083–4092, Jul. 2021.
[14] H. Chung et al., "Adaptive beamwidth control for mmWave beam tracking," *IEEE Commun. Lett.*, vol. 25, no. 1, pp. 137–141, Jan. 2021.